J. Phys. B: At. Mol. Opt. Phys. **40** (2007) 3211–3219 doi:10.1088/0953-4075/40/16/002

Two electromagnetically induced transparency windows and an enhanced electromagnetically induced transparency signal in a four-level tripod atomic system

Shujing Li, Xudong Yang, Xuemin Cao, Changde Xie and Hai Wang

The State Key Laboratory of Quantum Optics and Quantum Optics Devices, Institute of Opto-Electronics, Shanxi University, Taiyuan 030006, People's Republic of China

E-mail: wanghai@sxu.edu.cn.

Received 29 April 2007, in final form 10 July 2007
Published 3 August 2007
Online at stacks.iop.org/JPhysB/40/3211

Abstract

We present the experimental observations and theoretical calculations of two electromagnetically induced transparency (EIT) windows and an enhanced EIT signal in a four-level tripod system of D1 line of ^{87}Rb atoms. The two EIT dips produced by a strong coupling beam and a weak trigger beam were observed in the absorption spectrum of probe field, when the frequency detuning of the trigger beam was different from that of the coupling beam. When the frequency detuning of the trigger beam was near or equal to that of the coupling beam, the total depth of the EIT dip created by the coupling beam clearly became larger. The experimental measurements were in agreement with theoretical calculations.

(Some figures in this article are in colour only in the electronic version)

Since the early demonstrations of the electromagnetically induced transparency (EIT) phenomenon in various three-level atomic systems [1–3], many new EIT-related effects in various four- or five-level EIT systems have been theoretically and experimentally studied [4–16]. Harris *et al* [5] proposed to use an *N*-type EIT system to achieve a nonlinear two-photon absorption. Yan *et al* [6] have observed two-photon absorption via quantum interference in an *N*-type four-level system in cold Rb atoms. Jiang *et al* studied the modified EIT signal by optical pumping in an *N*-type four-level system in atomic vapor [8]. Recently, the EIT-related effects in a four-level tripod-type system have been extensively studied in theory [9, 10, 13–16]; these studies have shown that the four-level tripod EIT system can be used to obtain large cross-phase modulation [9], create double EIT windows [14], obtain a sub-Doppler and sub-natural narrowing of an absorption line [14], and store a light pulse in two channels [15]. In the experiment, Ham *et al* observed dark resonance switching among three-laser interactions in a four-level tripod EIT system [16].

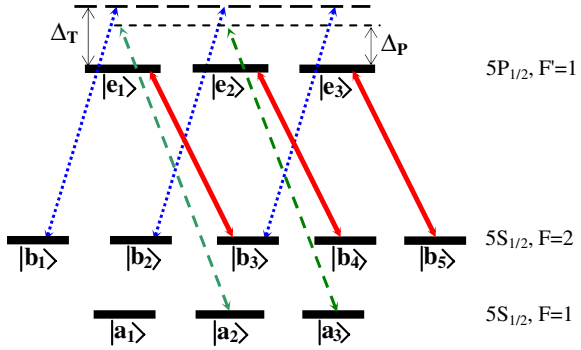

Figure 1. Relevant atomic energy level diagram of the D1 line in ^{87}Rb atom. Solid lines: transitions for the left-circularly polarized coupling beam; dashed lines: transitions for the left-circularly polarized probe beam; dotted lines: transitions for the right-circularly polarized trigger beam.

In this paper, we report theoretical calculations and experimental observations of two EIT windows and enhanced EIT signal in a four-level tripod system of D1 line of ^{87}Rb atoms. The relevant atomic levels in ^{87}Rb D1 line are shown in figure 1. We choose $5P_{1/2}$, $F' = 1$ to be the upper state $|e\rangle$ and $5S_{1/2}$, $F = 1, 2$ to be the lower states $|a\rangle$ and $|b\rangle$. The transition frequencies from atomic levels $|b\rangle$ to $|e\rangle$ and $|a\rangle$ to $|e\rangle$ are denoted as ω_{be} and ω_{ae}, respectively. The Zeeman sublevels of $5S_{1/2}$, $F = 1$ are denoted as $|a_i\rangle$ ($i = 1$–3 for $m = -1, 0, +1$), of $5S_{1/2}$, $F = 2$ are denoted as $|b_j\rangle$ ($j = 1$–5 for $m = -2, -1, 0, +1, +2$), of $5P_{1/2}$, $F' = 1$ as $|e_k\rangle$ ($k = 1$–3 for $m = -1, 0, +1$). We choose the probe beam (with frequency ω_P) to be as a left-circularly-polarized laser beam, coupling to the transitions from levels $|a_{i+1}\rangle$ to $|e_i\rangle$ ($i = 1, 2$). The coupling beam is a left-circularly-polarized laser beam (with frequency ω_C) driving the $|b_{j+2}\rangle$ to $|e_j\rangle$ transition ($j = 1, 2, 3$), the trigger beam is a right-circularly-polarized laser beam (with frequency ω_T) coupling to the $|b_k\rangle$ to $|e_k\rangle$ transitions ($k = 1, 2, 3$). In the present work, the theoretical model may be considered as two four-level tripod-type systems; one of them consists of levels $|a_2\rangle - |b_3\rangle - |b_1\rangle - |e_1\rangle$ and the other one consists of levels $|a_3\rangle - |b_4\rangle - |b_2\rangle - |e_2\rangle$. Actually, the trigger laser can also couple $|b_3\rangle$ to $|e_3\rangle$, and the coupling laser can couple $|b_5\rangle$ to $|e_3\rangle$, which leads to a six-level system $|a_2\rangle - |b_3\rangle - |b_1\rangle - |e_1\rangle - |e_3\rangle - |b_5\rangle$, not a four-level tripod system $|a_2\rangle - |b_3\rangle - |b_1\rangle - |e_1\rangle$. But in our experiment, the Rabi frequencies of trigger and probe beams are much smaller than that of coupling beam, thus most of the atoms in $F = 2$ level are prepared in $|b_1\rangle$ and $|b_2\rangle$ states. Under these conditions, the six-level system $|a_2\rangle - |b_3\rangle - |b_1\rangle - |e_1\rangle - |e_3\rangle - |b_5\rangle$ can be simplified into the four-level tripod system $|a_2\rangle - |b_3\rangle - |b_1\rangle - |e_1\rangle$. A similar simplification was made in [17, 18]. Since the magnetic field is close to zero in our experiment, the Zeeman sublevels $|a_1\rangle - |a_3\rangle$, $|b_1\rangle - |b_5\rangle$ and $|e_1\rangle - |e_3\rangle$ are degenerate. Thus we have $\omega_{a_2,e_1} = \omega_{a_3,e_2} = \omega_{ae}$, $\omega_{b_3,e_1} = \omega_{b_4,e_2} = \omega_{b_5,e_3} = \omega_{be}$ and $\omega_{b_1,e_1} = \omega_{b_2,e_2} = \omega_{be}$. The frequency detunings of the probe, the coupling and the trigger laser beams are defined as $\Delta_P = \omega_P - \omega_{ae}$, $\Delta_C = \omega_C - \omega_{be}$ and $\Delta_T = \omega_T - \omega_{be}$, respectively. Each tripod-type system can be viewed as two three-level Λ-type systems; one is coupled by the probe and trigger fields while the other is coupled by the probe and coupling fields. When the coupling detuning is different from the trigger detuning, i.e. $\Delta_C \neq \Delta_T$, the probe field will exhibit two EIT windows; one is created by the trigger beam at $\Delta_P = \Delta_T$, while the other is created by the coupling beam at $\Delta_P = \Delta_C$. In the resonant condition of probe, trigger and coupling fields ($\Delta_P = \Delta_T = \Delta_C = 0$), the two EIT windows will fuse into a single one created by the contribution of the combination of the coupling and the trigger fields. We

studied the above phenomenon in experiment and found that the experimental measurements were in agreement with theoretical calculations.

In the interaction picture and under rotating-wave approximations, the Hamiltonian for the practical systems can be described by

$$H_{\rm int} = H_{\rm int,1} + H_{\rm int,2}, \tag{1}$$

where

$$H_{\rm int,1} = \hbar\Delta_{\rm P}|{\rm e}_1\rangle\langle{\rm e}_1| + \hbar(\Delta_{\rm P} - \Delta_{\rm T})|{\rm b}_1\rangle\langle{\rm b}_1| + \hbar(\Delta_{\rm P} - \Delta_{\rm C})|{\rm b}_3\rangle\langle{\rm b}_3| - \frac{\hbar}{2}[\Omega_{\rm T1}|{\rm e}_1\rangle\langle{\rm b}_1| + \Omega_{\rm C1}|{\rm e}_1\rangle\langle{\rm b}_3| + \Omega_{\rm P1}|{\rm e}_1\rangle\langle{\rm a}_2| + {\rm c.c.}]$$

and

$$H_{\rm int,2} = \hbar\Delta_{\rm P}|{\rm e}_2\rangle\langle{\rm e}_2| + \hbar(\Delta_{\rm P} - \Delta_{\rm T})|{\rm b}_2\rangle\langle{\rm b}_2| + \hbar(\Delta_{\rm P} - \Delta_{\rm C})|{\rm b}_4\rangle\langle b_4| - \frac{\hbar}{2}[\Omega_{\rm T2}|{\rm e}_2\rangle\langle{\rm b}_2| + \Omega_{\rm C2}|{\rm e}_2\rangle\langle{\rm b}_4| + \Omega_{\rm P2}|{\rm e}_2\rangle\langle{\rm a}_3| + {\rm c.c.}]$$

are the Hamiltonians for the two four-level tripod-type systems $|{\rm a}_2\rangle - |{\rm b}_3\rangle - |{\rm b}_1\rangle - |{\rm e}_1\rangle$ and $|{\rm a}_3\rangle - |{\rm b}_4\rangle - |{\rm b}_2\rangle - |{\rm e}_2\rangle$, respectively. $\Omega_{{\rm P}i} = -\mu_{ei,ai+1}E_{\rm p}/\hbar$ $(i = 1, 2)$, $\Omega_{{\rm C}i} = -\mu_{ei,bi+2}E_{\rm c}/\hbar$ $(i = 1, 2)$ and $\Omega_{{\rm T}i} = -\mu_{ei,bi}E_{\rm T}/\hbar$ $(i = 1, 2)$ are the Rabi frequencies of the probe beam, coupling beam and trigger beam for various transitions among different Zeeman sub-levels, respectively. The dipole moments $\mu_{i,j}$ are different for different transitions since the Clebsch–Gordan coefficients of the various transitions in Zeeman sub-levels are different[1].

The evolution of the atomic variables in the system is governed by the master equation

$$\frac{\partial\tilde{\rho}}{\partial t} = -\frac{\rm i}{\hbar}[\tilde{H}_{\rm int}, \tilde{\rho}] + \left(\frac{\partial\tilde{\rho}}{\partial t}\right)_{\rm inc}, \tag{2}$$

where the first term results from the coherent interactions and the second term represents dampings due to spontaneous and other irreversible processes [19]. We write down the relevant density–matrix equations as follows:

$$\dot{\tilde{\rho}}_{{\rm a}_2{\rm a}_2} = \frac{\Gamma}{3}\tilde{\rho}_{{\rm e}_1{\rm e}_1} + \Lambda(\tilde{\rho}_{{\rm b}_1{\rm b}_1} + \tilde{\rho}_{{\rm b}_3{\rm b}_3}) - 2\Lambda\tilde{\rho}_{{\rm a}_2{\rm a}_2} - {\rm i}\left(\frac{\Omega_{\rm P1}}{2}\tilde{\rho}_{{\rm a}_2{\rm e}_1} - {\rm c.c.}\right),$$

$$\dot{\tilde{\rho}}_{{\rm b}_1{\rm b}_1} = \frac{\Gamma}{3}\tilde{\rho}_{{\rm e}_1{\rm e}_1} + \Lambda(\tilde{\rho}_{{\rm b}_3{\rm b}_3} + \tilde{\rho}_{{\rm a}_2{\rm a}_2}) - 2\Lambda\tilde{\rho}_{{\rm b}_1{\rm b}_1} - {\rm i}\left(\frac{\Omega_{\rm T1}}{2}\tilde{\rho}_{{\rm b}_1{\rm e}_1} - {\rm c.c.}\right),$$

$$\dot{\tilde{\rho}}_{{\rm b}_3{\rm b}_3} = \frac{\Gamma}{3}\tilde{\rho}_{{\rm e}_1{\rm e}_1} + \Lambda(\tilde{\rho}_{{\rm b}_1{\rm b}_1} + \tilde{\rho}_{{\rm a}_2{\rm a}_2}) - 2\Lambda\tilde{\rho}_{{\rm b}_3{\rm b}_3} - {\rm i}\left(\frac{\Omega_{\rm C1}}{2}\tilde{\rho}_{b_3e_1} - {\rm c.c.}\right),$$

$$\dot{\tilde{\rho}}_{{\rm e}_1{\rm e}_1} = -\Gamma\tilde{\rho}_{{\rm e}_1{\rm e}_1} - {\rm i}\left(\frac{\Omega^*_{\rm P1}}{2}\tilde{\rho}_{{\rm e}_1{\rm a}_2} + \frac{\Omega^*_{\rm T1}}{2}\tilde{\rho}_{{\rm e}_1{\rm b}_1} + \frac{\Omega^*_{\rm C1}}{2}\tilde{\rho}_{{\rm e}_1{\rm b}_3} - {\rm c.c.}\right),$$

$$\dot{\tilde{\rho}}_{{\rm a}_2{\rm e}_1} = ({\rm i}\Delta_{\rm P} - \gamma_{\rm e})\tilde{\rho}_{{\rm a}_2{\rm e}_1} + {\rm i}\frac{\Omega^*_{\rm p1}}{2}(\tilde{\rho}_{{\rm e}_1{\rm e}_1} - \tilde{\rho}_{{\rm a}_2{\rm a}_2}) - {\rm i}\frac{\Omega^*_{\rm T1}}{2}\tilde{\rho}_{{\rm a}_2{\rm b}_1} - {\rm i}\frac{\Omega^*_{\rm c1}}{2}\tilde{\rho}_{{\rm a}_2{\rm b}_3},$$

$$\dot{\tilde{\rho}}_{{\rm b}_1{\rm e}_1} = ({\rm i}\Delta_{\rm T} - \gamma_{\rm e})\tilde{\rho}_{{\rm b}_1{\rm e}_1} + {\rm i}\frac{\Omega^*_{\rm T1}}{2}(\tilde{\rho}_{{\rm e}_1{\rm e}_1} - \tilde{\rho}_{{\rm b}_1{\rm b}_1}) - {\rm i}\frac{\Omega^*_{\rm P1}}{2}\tilde{\rho}_{{\rm b}_1{\rm a}_2} - {\rm i}\frac{\Omega^*_{\rm c1}}{2}\tilde{\rho}_{{\rm b}_1{\rm b}_3},$$

$$\dot{\tilde{\rho}}_{{\rm b}_3{\rm e}_1} = ({\rm i}\Delta_{\rm C} - \gamma_{\rm e})\tilde{\rho}_{{\rm b}_3{\rm e}_1} + {\rm i}\frac{\Omega^*_{\rm C1}}{2}(\tilde{\rho}_{{\rm e}_1{\rm e}_1} - \tilde{\rho}_{{\rm b}_3{\rm b}_3}) - {\rm i}\frac{\Omega^*_{\rm P1}}{2}\tilde{\rho}_{{\rm b}_3{\rm a}_2} - {\rm i}\frac{\Omega^*_{\rm T1}}{2}\tilde{\rho}_{{\rm b}_3{\rm b}_1},$$

$$\dot{\tilde{\rho}}_{{\rm a}_2{\rm b}_1} = [{\rm i}(\Delta_{\rm P} - \Delta_{\rm T}) - \gamma_1]\,\tilde{\rho}_{{\rm a}_2{\rm b}_1} - {\rm i}\frac{\Omega_{\rm T1}}{2}\tilde{\rho}_{{\rm a}_2{\rm e}_1} + {\rm i}\frac{\Omega^*_{\rm p1}}{2}\tilde{\rho}_{{\rm e}_1{\rm b}_1},$$

[1] For details of the transition probabilities of D1 line in ^{87}Rb, see http://steck.us/alkalidata.

$$
\begin{aligned}
\dot{\tilde{\rho}}_{a_2b_3} &= [\mathrm{i}(\Delta_P - \Delta_C) - \gamma_2]\,\tilde{\rho}_{a_2b_3} - \mathrm{i}\frac{\Omega_{C1}}{2}\tilde{\rho}_{a_2e_1} + \mathrm{i}\frac{\Omega^*_{P1}}{2}\tilde{\rho}_{e_1b_3},\\
\dot{\tilde{\rho}}_{b_1b_3} &= [\mathrm{i}(\Delta_T - \Delta_C) - \gamma_3]\,\tilde{\rho}_{b_1b_3} - \mathrm{i}\frac{\Omega_{C1}}{2}\tilde{\rho}_{b_1e_1} + \mathrm{i}\frac{\Omega_{T1}}{2}\tilde{\rho}_{e_1b_3},\\
\dot{\tilde{\rho}}_{a_3a_3} &= \frac{\Gamma}{3}\tilde{\rho}_{e_2e_2} + \Lambda(\tilde{\rho}_{b_2b_2} + \tilde{\rho}_{b_4b_4}) - 2\Lambda\tilde{\rho}_{a_3a_3} - \mathrm{i}\left(\frac{\Omega_{P2}}{2}\tilde{\rho}_{a_3e_2} - \mathrm{c.c.}\right),\\
\dot{\tilde{\rho}}_{b_2b_2} &= \frac{\Gamma}{3}\tilde{\rho}_{e_2e_2} + \Lambda(\tilde{\rho}_{b_4b_4} + \tilde{\rho}_{a_3a_3}) - 2\Lambda\tilde{\rho}_{b_2b_2} - \mathrm{i}\left(\frac{\Omega_{T2}}{2}\tilde{\rho}_{b_2e_2} - \mathrm{c.c.}\right),\\
\dot{\tilde{\rho}}_{b_4b_4} &= \frac{\Gamma}{3}\tilde{\rho}_{e_2e_2} + \Lambda(\tilde{\rho}_{b_2b_2} + \tilde{\rho}_{a_3a_3}) - 2\Lambda\tilde{\rho}_{b_4b_4} - \mathrm{i}\left(\frac{\Omega_{C2}}{2}\tilde{\rho}_{b_4e_2} - \mathrm{c.c.}\right),\\
\dot{\tilde{\rho}}_{e_2e_2} &= -\Gamma\tilde{\rho}_{e_2e_2} - \mathrm{i}\left(\frac{\Omega^*_{P2}}{2}\tilde{\rho}_{e_2a_3} + \frac{\Omega^*_{T2}}{2}\tilde{\rho}_{e_2b_2} + \frac{\Omega^*_{C2}}{2}\tilde{\rho}_{e_2b_4} - \mathrm{c.c.}\right),\\
\dot{\tilde{\rho}}_{a_3e_2} &= (\mathrm{i}\Delta_P - \gamma_e)\tilde{\rho}_{a_3e_2} + \mathrm{i}\frac{\Omega^*_{p2}}{2}(\tilde{\rho}_{e_2e_2} - \tilde{\rho}_{a_3a_3}) - \mathrm{i}\frac{\Omega^*_{T2}}{2}\tilde{\rho}_{a_3b_2} - \mathrm{i}\frac{\Omega^*_{c2}}{2}\tilde{\rho}_{a_3b_4},\\
\dot{\tilde{\rho}}_{b_2e_2} &= (\mathrm{i}\Delta_T - \gamma_e)\tilde{\rho}_{b_2e_2} + \mathrm{i}\frac{\Omega^*_{T2}}{2}(\tilde{\rho}_{e_2e_2} - \tilde{\rho}_{b_2b_2}) - \mathrm{i}\frac{\Omega^*_{P2}}{2}\tilde{\rho}_{b_2a_3} - \mathrm{i}\frac{\Omega^*_{c2}}{2}\tilde{\rho}_{b_2b_4},\\
\dot{\tilde{\rho}}_{b_4e_2} &= (\mathrm{i}\Delta_C - \gamma_e)\tilde{\rho}_{b_4e_2} + \mathrm{i}\frac{\Omega^*_{C2}}{2}(\tilde{\rho}_{e_2e_2} - \tilde{\rho}_{b_4b_4}) - \mathrm{i}\frac{\Omega^*_{P2}}{2}\tilde{\rho}_{b_4a_3} - \mathrm{i}\frac{\Omega^*_{T2}}{2}\tilde{\rho}_{b_4b_2},\\
\dot{\tilde{\rho}}_{a_3b_2} &= [\mathrm{i}(\Delta_P - \Delta_T) - \gamma_1]\,\tilde{\rho}_{a_3b_2} - \mathrm{i}\frac{\Omega_{T2}}{2}\tilde{\rho}_{a_3e_2} + \mathrm{i}\frac{\Omega^*_{p2}}{2}\tilde{\rho}_{e_2b_2},\\
\dot{\tilde{\rho}}_{a_3b_4} &= [\mathrm{i}(\Delta_P - \Delta_C) - \gamma_2]\,\tilde{\rho}_{a_3b_4} - \mathrm{i}\frac{\Omega_{C2}}{2}\tilde{\rho}_{a_3e_2} + \mathrm{i}\frac{\Omega^*_{P2}}{2}\tilde{\rho}_{e_2b_4},\\
\dot{\tilde{\rho}}_{b_2b_4} &= [\mathrm{i}(\Delta_T - \Delta_C) - \gamma_3]\,\tilde{\rho}_{b_2b_4} - \mathrm{i}\frac{\Omega_{C2}}{2}\tilde{\rho}_{b_2e_2} + \mathrm{i}\frac{\Omega_{T2}}{2}\tilde{\rho}_{e_2b_4},
\end{aligned}
\tag{3}
$$

where the density-matrix elements $\rho_{\alpha i,\beta j} = \langle \alpha i|\hat{\rho}|\beta j\rangle$. α and β denote the levels a, b or e, and i, j stand for the subscripts of Zeeman sub-level. Γ is the spontaneous decay rate of the excited lever $|\mathrm{e}\rangle$ and $\gamma_\mathrm{e} = \Gamma/2$. γ_1, γ_2 and γ_3 are the dephasing rates for the two ground states $|\mathrm{b}_1\rangle - |\mathrm{a}_2\rangle$ and $|\mathrm{b}_2\rangle - |\mathrm{a}_3\rangle$, $|\mathrm{b}_3\rangle - |\mathrm{a}_2\rangle$ and $|\mathrm{b}_4\rangle - |\mathrm{a}_3\rangle$, $|\mathrm{b}_1\rangle - |\mathrm{b}_3\rangle$ and $|\mathrm{b}_2\rangle - |\mathrm{b}_4\rangle$, respectively. If the effects on the dephasing rates of the laser linewidth of the probe, trigger and coupling beams are not considered, we have $\gamma_1 = \gamma_2 = \gamma_3 = \Lambda$ (Λ is the decay rate due to atomic collisions). In the numerical calculations matching the experimental results, the decay rate γ_e and the dephasing rates γ_1, γ_2 and γ_3 should include the laser linewidth [20]. Thus, we changed the dephasing rates γ_1, γ_2, γ_3 and γ_e into the effective decay rates as follows:

$$
\gamma_1^\mathrm{E} = \gamma_1 + \delta\omega_\mathrm{P}/2 + \delta\omega_\mathrm{T}/2, \qquad \gamma_2^\mathrm{E} = \gamma_2 + \delta\omega_\mathrm{P}/2 + \delta\omega_\mathrm{C}/2,
$$
$$
\gamma_3^\mathrm{E} = \gamma_3 + \delta\omega_\mathrm{C}/2 + \delta\omega_\mathrm{T}/2, \qquad \gamma_\mathrm{e}^\mathrm{E} = \gamma_\mathrm{e} + \delta\omega_\mathrm{P}/2,
$$

where $\delta\omega_\mathrm{P}$, $\delta\omega_\mathrm{C}$, $\delta\omega_\mathrm{T}$ are the full linewidths of the probe, coupling and trigger lasers respectively. Considering the frequency shifts due to the Doppler effect, the frequency detunings of the probe, coupling and trigger beams will become $\Delta_\mathrm{P} \to \Delta_\mathrm{P} + \omega_\mathrm{P}(v/c)$, $\Delta_\mathrm{C} \to \Delta_\mathrm{C} + \omega_\mathrm{C}(v/c)$ and $\Delta_\mathrm{T} \to \Delta_\mathrm{T} + \omega_\mathrm{T}(v/c)$ [21], respectively, where v is the velocity of moving atoms. Since the frequencies of the three laser beams are about the same ($\omega_\mathrm{P} \approx \omega_\mathrm{C} \approx \omega_\mathrm{T}$), the first-Doppler broadening in two-photon frequency detunings $\Delta_\mathrm{P} - \Delta_\mathrm{T}$ and $\Delta_\mathrm{P} - \Delta_\mathrm{C}$ will be eliminated by co-propagating the probe, coupling and trigger beams through the four-level tripod atomic system.

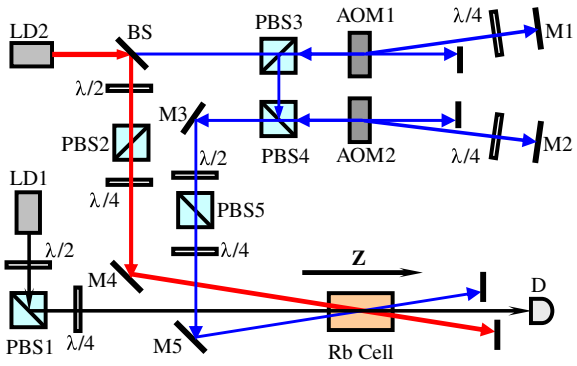

Figure 2. Experimental setup. LD1 and LD2: diode lasers; PBS1–PBS5: polarization cube beam splitters; AOM1 and AOM2: acousto-optical modulators; M1 and M2: mirrors with high reflectivity; $\lambda/2$ and $\lambda/4$: half-wave and quarter-wave plates; D: photodetector.

The susceptibilities of the probe field including the Doppler broadening effect are given by

$$\chi_{a_2,e_1} = -\frac{|\mu_{a_2,e_1}|^2}{\hbar\varepsilon_0\Omega_{p1}}\int_{-\infty}^{\infty}\tilde{\rho}_{a_2,e_1}N(v)\,dv, \tag{4a}$$

$$\chi_{a_3,e_2} = -\frac{|\mu_{a_3,e_2}|^2}{\hbar\varepsilon_0\Omega_{p2}}\int_{-\infty}^{\infty}\tilde{\rho}_{a_3,e_2}N(v)\,dv, \tag{4b}$$

where χ_{a_2,e_1} and χ_{a_3,e_2} correspond to the contributions of the two transitions $|a_2\rangle \rightarrow |e_1\rangle$ and $|a_3\rangle \rightarrow |e_2\rangle$, respectively. $N(v) = \frac{N_0}{u\sqrt{\pi}}\,e^{-v^2/u^2}$ is the Maxwellian velocity distribution, $u/\sqrt{2}$ is the root mean square atomic velocity and N_0 is the total atomic density of the vapor. The total susceptibility for the probe field can be written as

$$\chi = \chi_{a_2,e_1} + \chi_{a_3,e_2}, \tag{5}$$

The absorption coefficient for the probe beam is defined as

$$a = \omega_p n_0\,\mathrm{Im}[\chi]/c. \tag{6}$$

In the steady state, all values on the left-hand sides of equations (3) are equal to zero [22]. Thus, we can numerically calculate the absorption spectrum as a function of the frequency detuning of the probe field from equations (3)–(6).

Figure 2 depicts the experimental setup. LD1 (probe beam) and LD2 (coupling and trigger beams) are the frequency-stabilized diode lasers with the grating feedback. The probe beam is left-circularly polarized after passing through a polarization beam splitter (PBS1) and a quarter-wave plate. The LD2 laser beam is split into two parts by a beam splitter (BS); one of them serves as the coupling beam and the other one serves as the trigger beam. In the experiment, the LD2 laser is locked to the atomic transition frequency ω_{be}. For changing the frequency of the trigger beam around ω_{be}, we use two acousto-optical modulators AOM1 and AOM2 with the same center modulation frequency 200 MHz. The trigger beam first passes through a PBS3, AOM1 and a quarter-wave plate, and then is reflected back along the original way by a mirror M1. Double passing through the quarter-wave plate makes the polarization direction of the trigger beam rotate 90°, and then the trigger beam is reflected into PBS4 by

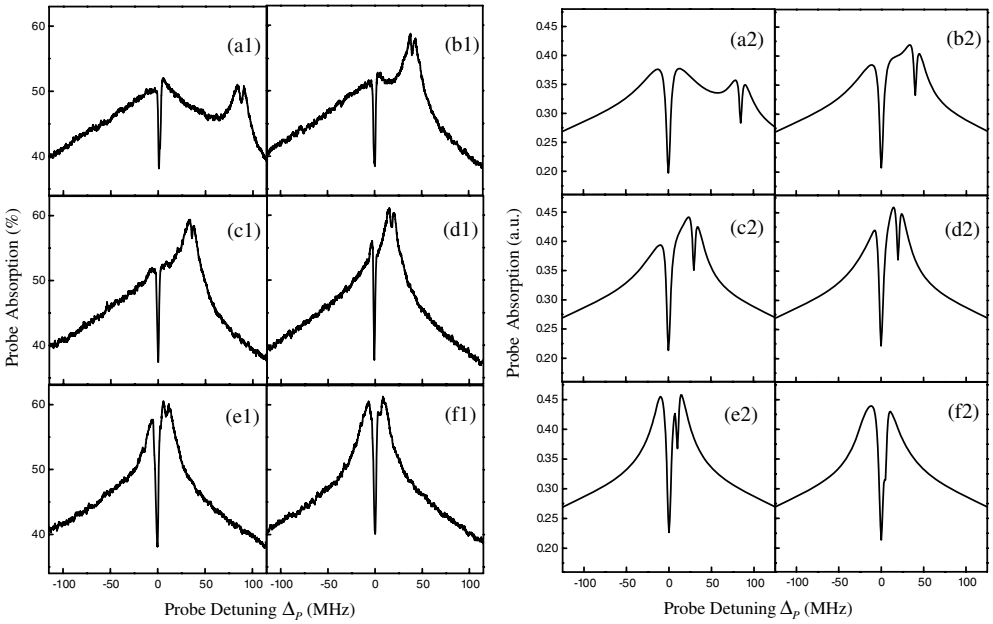

Figure 3. Probe absorption as a function of the probe frequency detuning. Parts (a1)–(f1) are experimental results for (a1) $\Delta_T = 85$ MHz, (b1) $\Delta_T = 40$ MHz, (c1) $\Delta_T = 30$ MHz, (d1) $\Delta_T = 20$ MHz, (e1) $\Delta_T = 10$ MHz, (f1) $\Delta_T = 5$ MHz; parts (a2)–(f2) correspond to theoretical results with parameters $\gamma_1 = 1.5$ MHz, $\gamma_2 = 1.5$ MHz, $\gamma_3 = 0.5$ MHz, $\gamma_e = 3.8$ MHz, $\Omega_C = 40$ MHz, $\Omega_P = 2.5$ MHz, $\Omega_T = 8$ MHz.

PBS3. We use the 1-order diffracted beam from AOM1, so the frequency of trigger beam is up-shifted by 400 MHz after it passes through AOM1 and goes back. The reflected trigger beam by PBS4 passes through another acousto-optical modulator AOM2 and a quarter-wave plate, and then is reflected back through them again. We use the -1-order diffracted beam from AOM2, so the trigger frequency is down shifted by 400 MHz, and then it regains the original frequency (ω_{be}). In the experiment, by changing the modulation frequency of AOM2 around its center frequency (200 MHz), we can tune the trigger frequency around the atomic transition frequency ω_{be} and fix it to the desired values. We use the method of double passing through AOM to prevent the deviation of trigger beam from its initial propagation direction during the modulation frequency of AOM2 being scanned. After the trigger beam passes through a polarization beam splitter (PBS5) and a quarter-wave plate, it becomes the right-circularly polarized, while the coupling beam is the left-circularly polarized beam. The coupling, trigger and probe beams co-propagate through a Rb vapor cell. The atomic cell is 5 cm long with magnetic shielding and its temperature is stabilized to 65 °C. The diameters of the coupling, trigger and probe beams are 1.5, 1.5, 1 mm at the cell center, respectively. The coupling beam and trigger beam are aligned at a small angle (about 2°) from the probe beam and three of them overlap well inside the Rb atomic cell. The input probe power is 5 μW (corresponding to the Rabi frequency of $\Omega_P = 2.5$ MHz) and its transmission is detected by detector D.

By keeping $\Delta_C = 0$ and scanning the probe frequency around the transition from level $5S_{1/2}$, $F = 1$ to level $5P_{1/2}$, $F' = 1$, we measured the absorption of probe beam versus the frequency detuning Δ_P for several different Δ_T. Figures 3(a1)–(f1) are the measured absorption spectra for $\Delta_T = 85$, 40, 30, 20, 10, 5 MHz, respectively. The powers of the coupling and trigger beams were set at 3 mW and 120 μW, corresponding to the Rabi

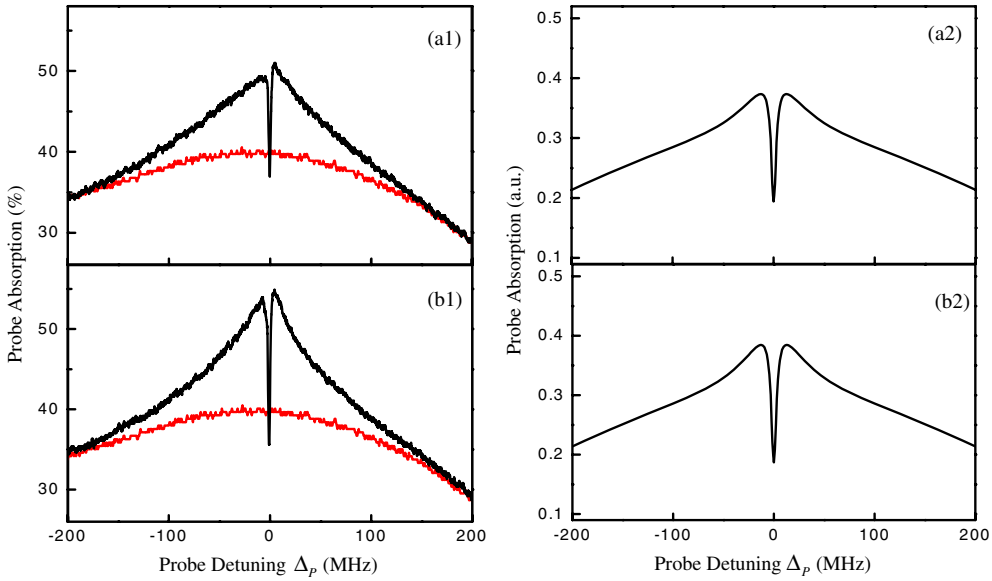

Figure 4. Probe absorption as a function of the probe frequency detuning at exact EIT resonance ($\Delta_C = \Delta_T = 0$). Parts (a1), (b1) are experimental results, the upper curve of (a1) is only with the coupling beam, (b1) is with both the coupling beam and trigger beam. The identical absorption (lower) curves of (a1), (b1) are with no coupling and trigger beams; parts (a2), (b2) are theoretical results with the same parameters as in figures 3(a2)–(b2).

frequencies of $\Omega_C = 40$ MHz and $\Omega_T = 8$ MHz, respectively. From figure 3, one can see that there are two EIT dips in the absorption spectra of the probe beam. The big one is produced by the stronger coupling beam which appears at two-photon resonance $\Delta_P = \Delta_C = 0$, while the small one is produced by the weaker trigger beam which appears at two-photon resonance $\Delta_P = \Delta_T$. The small EIT dip is in the center of a small domelike absorption curve; such a small domelike absorption curve is an increase in absorption due to optical pumping [23] of the trigger beam. Comparing figures 3(a1)–(f1), one can see that the height of the big EIT dip at $\Delta_P = 0$ obviously becomes larger when the small EIT dip at $\Delta_P = \Delta_T$ is close to it. The heights of EIT dip at $\Delta_P = 0$ in figures 3(e1), (f1) are about 1.45 times of that in figure 3(a1). It is noted that although the height of the big EIT dip becomes larger, the absorption at the top of the big EIT dip (figures 3(e1) and (f1)) does not obviously decrease.

Figures 3(a2)–(f2) plot the corresponding theoretical calculations of the probe absorption versus probe frequency detuning Δ_P for $\Delta_T = 85$, 40, 30, 20, 10 and 5 MHz, respectively. In the calculations, the Doppler effect and the laser linewidth have been taken into account. The linewidths of the two lasers used in our experiment are about 1.5 MHz, and the coupling and the trigger beams are taken from a same laser also, so we can consider the effective decay rates [20] $\gamma_1 = \gamma_2 \approx 1.5$ MHz and $\gamma_3 \approx 0.5$ MHz. The theoretical results clearly show the two EIT windows and that the total depth of the big EIT dip produced by the coupling beam (at $\Delta_P = 0$) becomes larger with the small EIT dip close to it, which are in good agreement with the experimental results as shown in figures 3(a1)–(f1).

Next, we study the enhanced EIT signal by the trigger beam under the exact EIT resonance conditions $\Delta_C = 0$ and $\Delta_T = 0$. The results are plotted in figure 4. The identical curves (lower curves) in figures 4(a1) and (b1) are the measured probe absorption as a function of the probe frequency detuning without the coupling and trigger beams. The upper curve in

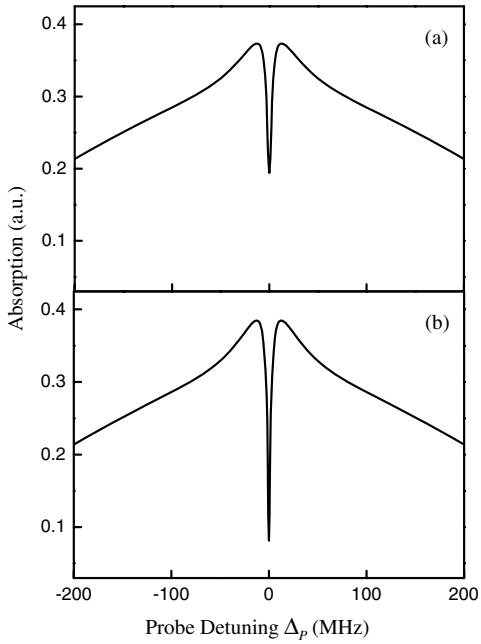

Figure 5. Theoretical results of probe absorption as a function of the probe frequency detuning at exact EIT resonance ($\Delta_C = \Delta_T = 0$). (a) EIT signal without the trigger beam and (b) EIT signal with the trigger beam. The parameters $\gamma_1 = 0.1$ MHz, $\gamma_2 = 1.5$ MHz, $\gamma_3 = 0.5$ MHz, $\gamma_e = 3.8$ MHz, $\Omega_C = 40$ MHz, $\Omega_P = 2.5$ MHz, $\Omega_T = 8$ MHz.

figure 4(a1) is the measured probe absorption when only the coupling beam of 3 mW is turned on. A clear EIT dip produced by the coupling beam appears at the center of the upper absorption curve. The increase in absorption background for the upper curve is due to the optical pumping of coupling beam. When the trigger beam with a power of 120 μW is turned on also, the total depth of the EIT dip becomes larger, as shown in figure 3(b1). Its depth increases to about 1.4 times of the original EIT dip depth (in figure 3(a1)), but the probe absorption at the peak of EIT is not clearly become smaller than that of original (figure 3(a1)), which partially results from the effect of the absorption background increase induced by optical pumping with the trigger beam turned on. Figures 4(a2) and (b2) plot the corresponding theoretical calculations of the probe absorption as a function of Δ_P with only coupling beam and with both coupling and trigger beams, respectively, on the resonance $\Delta_C = \Delta_T = 0$. The results show that the depth of EIT dip (as shown in figure 4(a2)) becomes larger with the trigger beam turned on (as shown in figure 4(b2)), and the absorption at EIT peak is decreased. This decrease is not observed in the experiment. To obtain the significant modification of the probe absorption at the EIT peak by the trigger beam, we calculate the probe absorption as the function of Δ_P with $\gamma_1 = 0.1$ MHz, all the other parameters are the same as that in figure 4. The results show that the EIT signal produced by the coupling beam without the trigger beam (figure 5(a)) becomes larger with the trigger beam (figure 5(b)), which means that the absorption at the EIT peak is greatly decreased if the trigger beam is turned on. By narrowing the linewidths of the probe and trigger lasers, one can decrease the effective decay rate γ_1, and then the more modification of the absorption of the probe field at EIT peak can be observed experimentally.

In summary, we have experimentally observed and theoretically calculated the two EIT windows and the enhanced EIT signal in a four-level tripod system of ^{87}Rb atoms. A big

EIT dip produced by a strong coupling beam and a small EIT dip produced by the weak trigger beam were observed in the absorption spectrum of the probe field when the frequency detunings of the trigger beam are different from that of the coupling beam. If the frequency of the trigger beam is far away from that of the coupling beam, the big EIT dip will not be affected by the small EIT dip; however, if the frequency of the trigger beam is close to or equals that of the coupling beam, the total depth of the big EIT dip becomes larger. The calculated results also show that the more modification of the absorption at the EIT peak resulting from the trigger beam can be obtained in the experiment by narrowing the linewidths of the probe and the trigger lasers. The modification of the absorption of the probe field near EIT dip by the trigger beam can be considered as the third-order nonlinear absorption, which indicates that the system exists a Kerr-type cross-phase modulation in terms of the Kramers–Kronig relation [24].

Acknowledgments

We acknowledge funding supports by the National Natural Science Foundation of China (nos 60325414, 60578059, RGC60518001), 973 Program (no 2006CB921103) and the CFKSTIP (Ministry of Education of China, no 705010).

References

[1] Harris S E 1997 *Phys. Today* **50** 36
[2] Boller K J, Imamoglu A and Harris S E 1991 *Phys. Rev. Lett.* **66** 2593
[3] Gea-Banacloche J, Li Y, Jin S-Z and Xiao M 1995 *Phys. Rev.* A **51** 576
[4] Schmidt H and Imamoglu A 1996 *Opt. Lett.* **21** 1936
[5] Harris S E and Yamamoto Y 1998 *Phys. Rev. Lett.* **81** 3611
[6] Yan M, Rickey E G and Zhu Y 2001 *Opt. Lett.* **26** 548
[7] Kang H and Zhu Y 2003 *Phys. Rev. Lett.* **91** 093601
[8] Jiang W, Chen Q, Zhang Y and Guo G-C 2006 *Phys. Rev.* A **73** 053804
[9] Rebic S, Vitali D, Ottaviani C, Tombesi P, Artoni M, Cataliotti F and Corbalán R 2004 *Phys. Rev.* A **70** 032317
[10] Petrosyan D and Malakyan Y P 2004 *Phys. Rev.* A **70** 023822
[11] Petrosyan D and Kurizki G 2002 *Phys. Rev.* A **65** 033833
[12] Joshi A and Xiao M 2005 *Phys. Rev.* A **71** 041801
[13] Paspalakis E and Knight P L 2002 *Phys. Rev.* A **66** 015802
[14] Goren C, Wilson-Gordon A D, Rosenbluh M and Friedmann H 2004 *Phys. Rev.* A **69** 063802
[15] Raczynski A, Rzepecka M, Zaremba J and Zielinska-Kaniasty S 2006 *Opt. Commun.* **260** 73
[16] Ham B S and Hemmer P 2000 *Phys. Rev. Lett.* **84** 4080
[17] Phillips D F, Fleischhauer A, Mair A and Walsworth R L 2001 *Phys. Rev. Lett.* **86** 783
[18] Wang Z-B, Marzlin K-P and Sanders B C 2006 *Phys. Rev. Lett.* **97** 063901
[19] Ling H Y, Li Y Q and Xiao M 1996 *Phys. Rev.* A **53** 1014
[20] Lu B, Burkett W H and Xiao M 1997 *Phys. Rev.* A **56** 976
[21] Wang H, Goorskey D and Xiao M 2002 *J. Mod. Opt.* **49** 335
[22] Wu J-H, Cui C-L, Ba N, Ma Q-R and Gao J-Y 2007 *Phys. Rev.* A **75** 043819
[23] Ye C Y and Zibrov A S 2002 *Phys. Rev.* A **65** 023806
[24] Yariv A 1975 *Quantum Electronics* 2nd edn (New York: Wiley) p 154